Ionizing radiation hardness tests of GaN HEMTs for harsh environments

Alexis C. Vilas Bôas [a],[*], M.A.A. de Melo [a], R.B.B. Santos [a], R. Giacomini [a], N.H. Medina [b], L.E. Seixas [c], S. Finco [c], F.R. Palomo [d], A. Romero-Maestre [d], Marcilei A. Guazzelli [a]

[a] Centro Universitário FEI, São Bernardo do Campo, Brazil
[b] Instituto de Física da Universidade de São Paulo, São Paulo, Brazil
[c] Centro de Tecnologia da Informação Renato Archer, Campinas, Brazil
[d] Universidad de Sevilla, Sevilla, Spain

ARTICLE INFO

ABSTRACT

The COTS power transistors based in GaN were exposed to TID effects by 10-keV X-rays. These HEMTs were tested in the On- and Off-state bias conditions. Switching tests were performed before and after irradiation steps. The devices were characterized at temperatures ranging from $-50\,°C$ to $+75\,°C$. The results indicate that the GaN-technology is a great candidate to be used in harsh environments, because the tested devices have presented an expressive recovery of its parameters of V_{th}, gm_{max} and switching times, after accumulation of 350 krad of TID.

1. Introduction

Since the 90s, new generation of semiconductor components, the High-electron-mobility transistor (HEMT), is under study and evaluation thanks to the advent of wide bandgap (WBG) materials such as GaN, with a bandgap of 3.4 eV [1–4]. HEMT devices incorporate heterojunctions where electrons are confined in a quantum well to avoid the impurity scattering, which is a drawback of traditional MOS devices for high frequency, low noise, and high-power applications [1,2]. These devices are also known as Two-Dimensional Electron Gas Field-Effect Transistor (TEGFET).

In recent years, there have been major advantages in the use of power devices based on GaN technologies. The availability of qualified commercial devices and the fall in price with increased production have led to the intensification of the use of these power devices. As the adoption of WBG devices increases, market dynamics is changing and enabling the use of these power devices in emerging applications that were beyond the realm of Si which presents a bandgap of about 1.1 eV [5].

AlGaN/GaN HEMT can operate at very high frequencies and high temperatures with satisfactory performance as well as possess high breakdown strength and high electron velocity in saturation [2,6,7,8]. A conventional GaN-based HEMTs have the layered structure as shown in Fig. 1. Rather electrons come from surface states due to the spontaneous polarization found in wurtzite-structured GaN. This accumulation of free carrier leads to high carrier concentration at the interface, creating a two-dimensional electron gas (2DEG) channel [6,9–11].

The characteristics of GaN-based power transistors are required for a number of important functions, such as the transmission of signals over long distances or at high-end power levels such as radar and satellite [4]. Faced with the possibility of more robust devices as the effects of ionizing radiation, this technology can reduce the need to replace detectors based on Si, in applications for example at the CERN Large Hadron Collider (LHC), which currently detectors are replaced at least once per year [3].

In view of the various applications that can be improved with the use of GaN HEMT, being able to be exposed to the effects of ionizing radiation, it is very important to know the behavior of these new technological devices in relation to the accumulation of the Total Ionizing Dose (TID).

This work shows a systematic study of a commercial-off-the-shelf (COTs) GaN HEMT, GS61008T, enhancement-mode GaN transistor, regarding the TID radiation effects using a 10-keV X-ray source with a dose rate of 114 krad (Si)/h (1 rad $= 10^{-2}$ Gy) [12]. The GS61008T is a transistor that offers very low junction-to-case thermal resistance for demanding high power applications. These features combine to provide very high efficiency power switching [12].
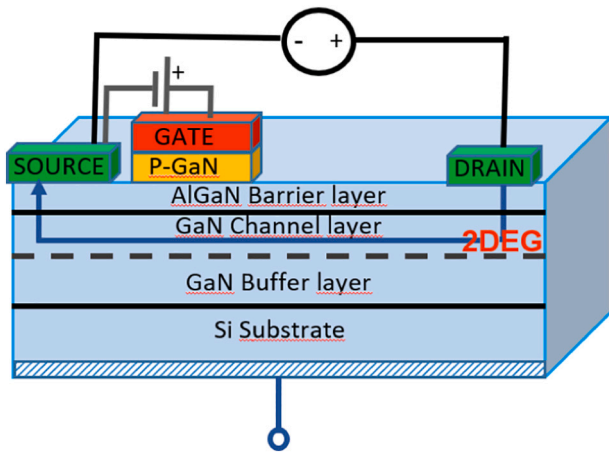
Fig. 1. Schematic diagram for a conventional gate injected AlGaN/GaN HEMT structure, showing the two-dimensional electron gas (2DEG) as an arrow near the GaN/AlGaN interface, adapted of [9,11].

2. Radiation damage

In a hostile environment, an electronic device may be exposed to the effects of interactions with charged particles (protons, electrons and heavy ions), high energy photons (gamma and X-rays), and neutrons (avionics) [13]. All these charged particles and photons, when interacting with the semiconductor devices, generate damages due to the cumulative effects. The magnitude of this damage is related to the Total Ionizing Dose (TID) absorbed by each electronic device, which is an effect that refers to the amount of energy absorbed by the material [13,14]. That's why it is always necessary to test in advance the electronic components that will be exposed to environments with ionizing radiation as to the radiation dose accumulated in the device [14,15].

The TID effects can be generated when a photon interacts with the material creating electron-hole pairs, momentarily or permanently modifying its conductivity. Since the mobility of the holes is much smaller than the electrons, an accumulation of charges may occur in certain regions, changing the basic operating characteristics of the electronic device [13–15].

GaN WBG material presents strong atomic bonding, making the resistance to ionizing radiation an intrinsic property of this material [2,3]. The strength of this bonding force is the energy required to displace an atom from its lattice position and it is called the atomic displacement energy [3,16,17,18,19]. This energy is directly correlated with the difficulty in creating crystalline network displacements, representing a resistance to the damages caused by radiation in a semiconductor.

The modification of characteristic parameters in a semiconductor depends not only on the intrinsic properties of the material, but on the type of interaction with the radiation, the accumulated dose and energy transferred, as well as the density of carriers, impurities and defect states [20–22].

Other studies about the tolerance to TID effects in GaN-based devices using different radiation sources were performed [23–27]. M.J. Martinez et al. observed the tolerance to TID effects of $Al_xGa_{1-x}N$ transistors in different experimental conditions, using 2.5 MeV proton beam, with a total fluence of 10^{14} protons/cm^2 achieving 131 Mrad total dose [23]. X. Sun et al. performed a comparative study between conventional and AlGaN/GaN HEMTs with a dose rate of 31.5 krad/min 10-keV X-ray up to about 1.0 Mrad [24]. R. Jiang et al. verified small changes in GaN-based HEMTs exposed to different sources of electromagnetic radiation (10-keV X-ray with 510 rad(SiO$_2$)/s and ^{137}Cs gamma source at a rate of 0.070 rad(SiO$_2$)/s) for TID effects [25]. A. Lidow et al. did experiments using ^{60}Co gamma-ray source with 96 rad/s accumulating a total dose of about 1.0 Mrad, proving the tolerance of GaN-based devices

[26] and R.D. Harris et al. submitted GaN-based devices to 55 MeV proton beam observing no TID effects [27].

3. Methodology

This work was carried out with a total of 6 samples of the transistor GS61008T (from the same batch), 4 of which were destined for the irradiation tests, followed by the temperature test, and 2 samples destined for the switching test.

The characteristic curves of drain current (I_d) as a function of drain voltage (V_d) were acquired with V_d ranging from 0 up to 15 mV and V_g ranging from 1 up to 3.0 V; I_d as a function of gate voltage (V_g) were traced for Vg ranging from 0 up to 3.0 V and drain voltage $V_d = 10$ mV. In these ranges it is possible to verify the behavior of the device at low currents (approximately 2.0 A), very sensitive to the effects of TID. In addition, a test was performed to verify the switching speed of the devices before and after accumulating radiation dose.

3.1. Irradiation tests

Fig. 2 shows the schematic diagram for the total experimental procedures of the radiation, switching and temperature tests. Electrical characterization was performed on each of the six steps and during irradiation process. Switching tests were performed before and after irradiation.

In order to measure the sensitivity of the COTS GaN-on-silicon transistor due to TID, an XRD-6100 (Shimadzu) X-ray diffractometer setup was used. The devices under test (DUTs) of the same batch were exposed to 10 keV X-ray source, maintaining the procedure of the irradiation steps and electrical measurements [20–22,28–30]. In fact, for TID effects, a 10-keV X-ray radiation is a very convenient source of radiation owing to its higher charge yield compared to protons, alpha particles and heavy ions [20,29]. Although the effects caused by 10-keV X-ray photons and 1.25 MeV of ^{60}Co are comparable, they are generated by different physical mechanisms resulting from the interaction of radiation with matter [20,29].
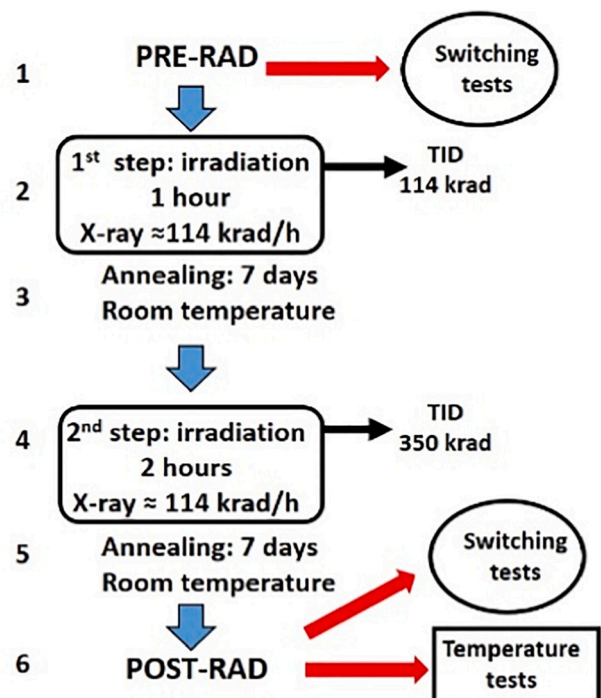

Fig. 2. Schematic diagram for the experimental procedure to verify the electrical characterization due to TID.

X-ray sources are very versatile for studying radiation effects in electronic devices since it is possible to modify the X-ray tube current, bias and the source-device distance, in order to choose an adequate dose rate.

The device was analyzed both in the On- and in the Off-state bias-conditions. For characterizations to be performed before, during and after irradiation, a portable National Instruments PXI platform was used [28].

All measurements were performed in controlled temperature of 21 °C (room temperature – RT). The devices were characterized before, during and after exposure to X-ray TID at a dose rate of about 114 krad (Si)/h and irradiated in two different approaches: I - in a 1st step the transistors were exposed to X-rays for 1 h; following this step, there was an intermediate step during which the devices were kept for a week at RT for charge stabilization into device; II - in the 2nd step, the devices were irradiated for approximately 2 h, reaching TID about 350 krad (Si).

3.1.1. X-ray dosimetry

Standard test procedure states that the DUT incident radiation must be characterized in terms or radiation energy and dose rate [31,32]. In this work the X-ray effective energy was determined using the half-value layer procedure, where aluminum thin foils were placed in front of X-ray radiation spectrum, emitted by a 20 kV copper X-ray source, in order to measure its half-layer value. This quantity was estimated considering the aluminum mass attenuation coefficient [20,21,33]. The result indicated that, applying 20 kV in the X-ray tube, the whole X-ray spectrum can be characterized by a monoenergetic 10-keV effective energy photon beam.

To check the spatial homogeneity of the beam, radiographic films exposed to different dose rates and distances in relation to the X-ray source were used. After each exposure, field radiation measurements were made using an appropriated densitometer [34]. In this way, it was possible to carry out radiation dose rate measurements, ensuring that the ionizing chamber was fully immersed in a homogeneous radiation field. The film exposures were performed for X-ray tube currents ranging from 2 mA to 40 mA, at different distances.

In order to determine the dose rate, a calibrated RADCAL 10X6-0.6 ionization chamber, with a rate range from 20 μR/s to 133 R/s (200 nGy/s to 1.17 Gy/s), a calibration accuracy of 4%, using ^{60}Co source, with an energy dependence of about 5% in an energy range from keV to MeV, was used. These measurements were performed in a controlled pressure and temperature environment [35,36]. If an accurate dose rate measurement is performed at a specific beam distance, and considering that the photon fluence is inversely proportional to the square of the distance from the source, it is possible to estimate the dose rate in positions closer to the X-ray source [35]. Dosimetry and monitoring techniques for total ionizing dose (TID) testing of electronics devices are well described in Ref. [34].

The ionization chamber provides results in air kerma (kinetic energy released per unit of mass) and absorbed dose [35]. The dose rate in air, D_{Air}, allows to estimate the dose rate in any material, for example, in Si, for the same exposure, through a conversion factor [33,34]. For the same irradiation condition, the relationship between the values of the absorbed dose in Si and in air, can be expressed by:

$$D_{Si} = D_{Air} \frac{(\mu_{en}/\rho)_{Si}}{(\mu_{en}/\rho)_{Air}} \tag{1}$$

where (μ_{en}/ρ) is the mass energy absorption coefficient of air or Si.

3.2. Switching tests

GaN-based inverters have been investigated to greatly help save energy in the future as an indispensable power switching system. The tests were performed in two frequency ranges: 100 Hz and 100 kHz. The measurement was performed by an R&S oscilloscope of 1 GHz, 10 GSa/s

and impedance Z = 1 MΩ, using a RT-ZP10 probe, 10:1, 500 MHz, 10 MΩ, 9.5 pF.

One of the main parameters that can affect the performance of the device during switching is the time interval that it spends for the On- to Off-state change, characterizing the fall time (t_f), and the time from Off- to On-state, the rise time (t_r). These parameters, obtained by exposing these GaN-based devices to the effects of ionizing radiation, can provide information on the reliability of its use in harsh environments. In order to verify the behavior of the device in operation, switching tests were performed before and after undergoing TID effects.

3.2.1. 100 Hz frequency

The experiment consisted in exciting the gate of the GaN-transistor with a square waveform with f = 100 Hz and observing the rise and fall times. The deformation of the waveform of the drain-to-source current was observed through the spectral analysis of the signal, using a rectangular Fourier Transform (FFT – Fast Fourier Transform). The circuit used to perform this test is shown in Fig. 3. The measurement was performed by an oscilloscope of 1 GHz, 10 GSa/s and impedance Z = 1 MΩ. The Square waveform generator used in the gate was NI PXI-5406 ($V_{GF} \pm 6$ V) along with the voltage source DC voltage source for drain NI PXI-4130 ($V_F = 100$ mV). Through a shunt ($R = 0.1$ Ω) connected to the source, the voltage is read at its terminals, making it possible to determine the current.

3.2.2. 100 kHz frequency

The experiment consisted in exciting the gate of the GaN-transistor with a square waveform with f = 100 kHz and observing the rise and fall times. To drive the device gate, a GaN gate driver, provided by GaN Systems, was used. It was implemented through an evaluation board, model GS61008P-EVBHF [37]. A gate driver is a power amplifier that accepts a low-power input from a controller IC and produces a high-current drive for the gate of a high-power transistor, such as an IGBT or power MOSFET. The circuit used to perform this test is shown in Fig. 4. A Square waveform generator was used in the gate ($V_{GF} = 0$ to 3 V) along with the DC current source for drain ($I = 1$ A; $V_F = 200$ mV). Through a shunt ($R = 0.1$ Ω) connected to the drain, the drain current was measured.

3.3. Temperature-induced parametric variation hardness assessment

In order to evaluate the temperature robustness of this GaN power-transistor with accumulated TID of 350 krad (Si) in the On- (biased) and Off-state, after reaching a stable state by room-temperature annealing (RTA), the DUTs were characterized in five different temperatures: −50 °C, −25 °C, 0 °C, 21 °C, 50 °C and 75 °C, since preliminary results suggested that, after being subjected to the effects of TID, the devices are more susceptible to parametric variation induced by
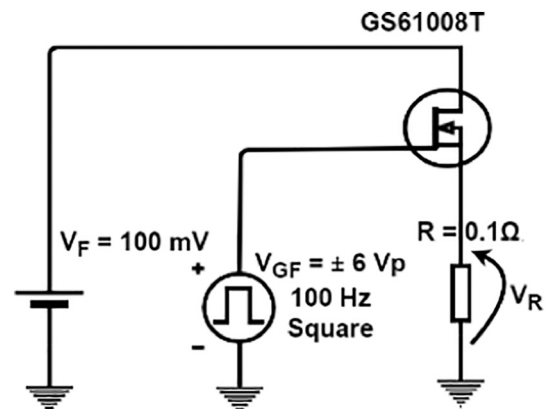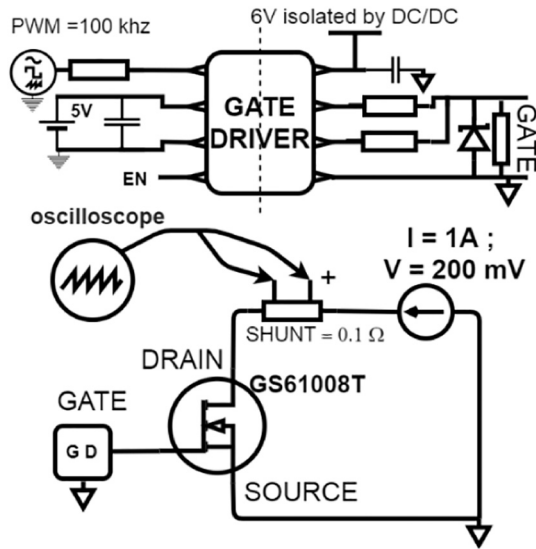

Fig. 3. Switching test circuit.

Fig. 4. Switching test circuit, composed by an isolated circuit, containing a DC/DC converter, and a gate driver ready to GaN technology. Circuit implemented through GS61008P-EVBHF evaluation board by GaN Systems.

Fig. 5. On-state (black points) and Off-state (red points) ΔV_{th} values for the first and second irradiation steps. (For interpretation of the references to colour in this figure legend, the reader is referred to the web version of this article.)

temperature effects [3,22,24].

Temperatures were maintained by a closed cycle cryostat (an ARS DE-202 cold head with an ARS 2HW compressor and a Lakeshore temperature controller). The DUTs were subjected to an NI LabVIEW-based automatic temperature control system, which allowed acquiring the I_d-V_g and the I_d-V_d characteristic curves for each temperature.

4. Experimental results and discussion

In this work we evaluated the parameters that are altered by TID effects and that govern the functionality of the DUTs. The values of the threshold voltage V_{th}, the transconductance gm, the currents I_{on} and I_{off}, were determined with the power devices in the On- and Off-state bias-conditions. Small changes in the output waveform were also observed when working as a power switch. The reference values obtained before the irradiation steps were: $V_{th} = (1.98 \pm 0.02)$ V, while the maximum transconductance $gm_{max} = (638 \pm 62)$ mS at $V_g = 1.72$ V. The gate leakage current was monitored along the characterization process, but no dependence on irradiation dose was observed.

4.1. DUT analysis

Figs. 5 and 6 show On- (black points) and Off-state (red points) for ΔV_{th} and Δgm_{max} values, respectively, measured by the second and first derivative method of the characteristic curves of I_d as a function of V_g obtained before, during and after the irradiation process. The dashed line indicates that annealing occurred in room temperature during 7 days between the two steps of the irradiation processes. After accumulating TID of 350 krad, the devices stabilized after one week, in the values circled in the graph. It is important to note that the worst effects due to radiation occur during and shortly after the DUTs have their behavior altered by the charges trapped in the device. After 7-day at RTA, the devices stabilize at values close to those of reference. However, it is noticeable that the DUT in the Off-state presented greater variations of ΔV_{th} than when it was in the On-state.

The greatest shift in V_{th} occurs at the beginning of the irradiation process, that is, regardless of being biased (On-) or unbiased (Off), the effects of TID saturate rapidly. This is an indication that this technology has few defect states for trapping positive charges. After RTA, with accumulated TID of 114 krad, the device shows total recovery of V_{th}, that can be caused by release of trapped holes in the AlGaN layer, and/or
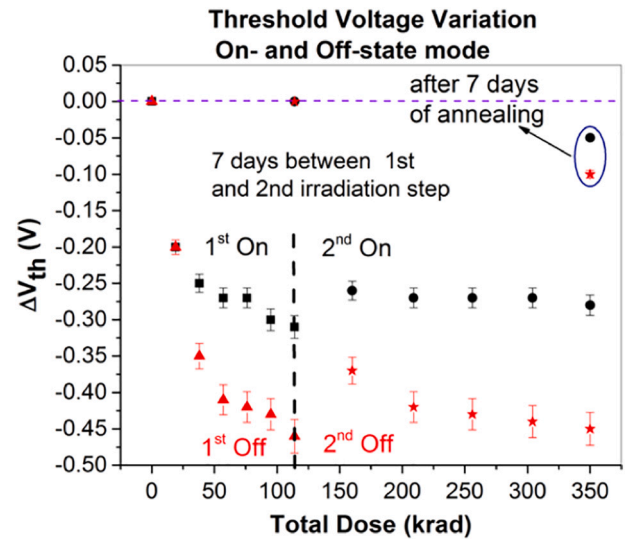

Fig. 6. On-state (black points) and Off-state (red points) Δg_m values for the first and second irradiation steps. (For interpretation of the references to colour in this figure legend, the reader is referred to the web version of this article.)
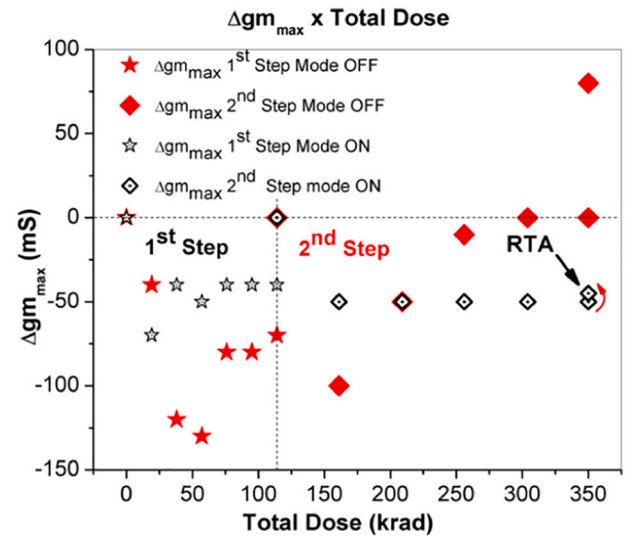
their neutralization by electrons from the channel. During the 2nd irradiation step the behavior of the devices are similar to the first step. After RTA having accumulated 350 krad, the recovery of V_{th} is not total, demonstrating that some charges were retained in the material traps, not having energy enough to escape.

Confirming the DUTs behavior due to V_{th} shifts, there is a small decrease in the gm_{max}, mainly during the irradiation process, compatible with current increase and decrease in the electron gas mobility of the channel. The lower the value of the transconductance, the less effective the gate voltage when controlling the drain current. That is, the positive charges trapped in the AlGaN modify the electric field, increasing the electron density in the conduction region, decreasing the mobility. Acquiring stability due to the RTA after the first step (114 krad TID), a regeneration of the mobility occurs, confirming a considerable recovery of the electrical characteristics.

After 2nd step, although the value of gm_{max} with TID of 350 krad, after 7 days RTA, for off mode, presented a value above the initial

reference value, all other values found indicate a small decrease of gm_{max} in both on and off state, showing better recovery of this parameter, after irradiated, in the off state.

The device irradiated with bias stabilized with the value slightly less. On- (black points) and Off-state (red points) Δg_m values measured by the first derivative method of the characteristic curves of I_d as a function of V_g obtained before, during e after the irradiation process can be seen in Fig. 6. Other results regarding shifts of the threshold voltage and transconductance after the first and second irradiation steps can be seen elsewhere [38].

Table 1 presents Δgm_{max} of the maximum transconductance as a function of the accumulated dose for transistors irradiated in On- and in Off-state mode, for the two-irradiation step. As shown in Fig. 6, shifts in the maximum transconductance were more pronounced when the transistor was irradiated in Off-state, presenting a final positive shift much higher than negative shift observed in On-state mode.

After the entire two-step irradiation process, the off-state current I_{off} increased slightly in the On-mode, signalling an increased power consumption when the device is switched off, and the saturation current I_{on} presented a slightly decrease in both cases. In the sum of the results obtained for the relation between I_{off} and I_{on}, it is possible to affirm that the effects of the radiation would not alter the functionality of this device COTS can be found in the paper [37].

Due to the decrease in the electron gas mobility inside the device channel, as a result of the effects of radiation, the maximum transconductance (gm_{max}) also decreases [38]. Both the rise and fall times depend directly on such parameter, therefore, with the interactions of the radiation, the switching times must rise [1,2,21,30,38].

4.2. Switching results for 100 Hz

In Fig. 7 the behavior of the square pulse used in the 100 Hz frequency switching test before and after each irradiation step is shown. The experimental data present a slight increase in the height of the pulse, and small changes in its shape, subtly altering the rise and fall time which define the switching power. Graphically, these times were extracted analyzing the interval between 10% and 90% of the monitored current during the switching response, resulting $t_r = (330 \pm 7)$ µs in all steps of the irradiation except in the post-1st rad (red pulse) where $t_r = (400 \pm 8)$ µs. On the other hand, no significant change was observed in fall time, which is very fast in comparison with the rise time: $t_f = (20.0 \pm 0.5)$ µs.

It is worth noting that there is an increase of the current level. This can be understood, considering that the threshold voltage is decreased after irradiation, so the gate overvoltage ($V_{gs} - V_{th}$) becomes greater, increasing the drain current.

In Fig. 8, the rectangular Fourier Transform (FFT) of these pulses, points the changes suffered due to the TID effects. A slight increase of magnitude in harmonics peaks of higher frequencies and the narrowing in the width.

Although these changes in the FFT are observed, their magnitudes do not appear to imply significant distortions during the functionality of this COTS based in GaN as a power key. No noteworthy change in

Table 1
Maximum transconductance with respect to the reference value before and after each irradiation step, in On- and Off-state mode.

TID	STEP	Δgm_{max} (S) On-state	Δgm_{max} (S) Off-state
Post-rad (114 krad)	First	−0.040	−0.070
Post 7-days RTA[a]		0.000	0.000
Post-rad (350 krad)	Second	−0.050	0.000
Post 7-days RTA[a]		−0.045	0.080

[a] RTA: room-temperature annealing.
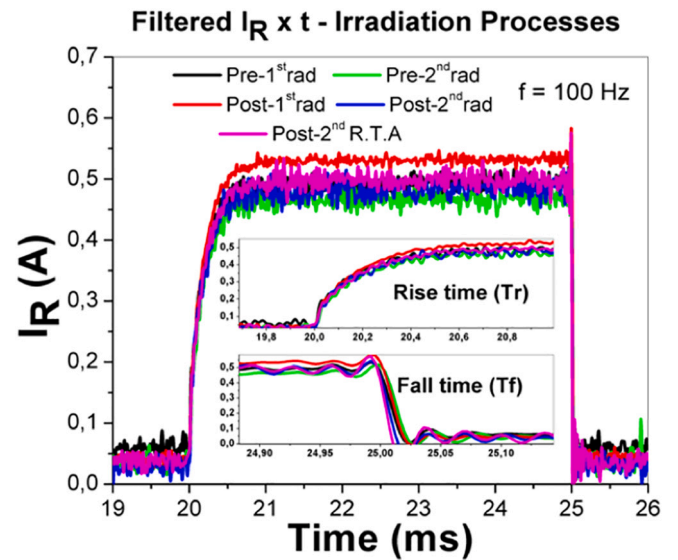
Fig. 7. Behavior of the square pulse used in the switching test before and after each irradiation step.
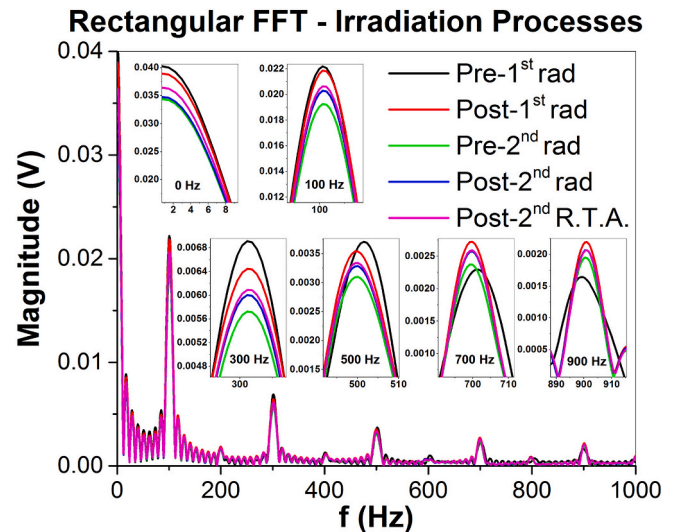
Fig. 8. *Fourier* Transformed to the square -wave signal used in the switching test, before and after TID effects.

device's response to irradiation was observed as a function of the test current level. Also, for lower currents, the experimental setup is less affected by the switching noise coming from the power circuitry external to the device under test, resulting in more accurate results. For this reason, the analysis was performed using low test currents.

4.3. Switching results for 100 kHz

In Fig. 9 the behavior of the square pulse used in the high frequency switching test before radiation and after room temperature annealing is shown.

In the experimental data, apart from the noise, it is observed that the duration of the rising and falling time is longer in the irradiated devices, as expected, due to the dynamic loading and unloading of traps caused by radiation in the 2DEG, which defines the degradation in the switching power. Graphically, these times were extracted analyzing the interval between 10% and 90% of the monitored current during the switching response. Pre-radiation rise and fall times were respectively
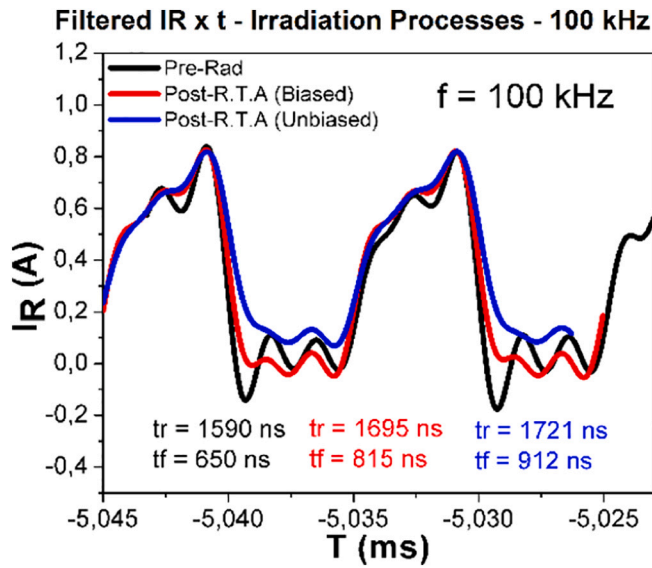
Fig. 9. Behavior of the square pulse used in the high frequency switching test before radiation and after room temperature annealing.

$t_r = (1.59 \pm 0.24)$ μs, $t_f = (0.650 \pm 0.097)$ μs. The radiation effects once again presented to be more pronounced in the Off-state mode, where $t_r = (1.72 \pm 0.26)$ μs, $t_f = (0.91 \pm 0.14)$ μs and On-state mode which had $t_r = (1.70 \pm 0.25)$ μs and $t_f = (0.82 \pm 0.11)$ μs. On the other hand, the blue curve, On-state (unbiased) did not show the complete recovery of the zero state, evidencing an increase of power losses.

4.4. Temperature-induced parametric variation hardness assessment results

The devices were subjected to several controlled temperatures to evaluate the stability of the device after entrapment of the charges by TID of 350 krad. In Fig. 10 the observed variations of the parameters V_{th} and gm_{max} as a function of temperature are shown. While I_{off} and I_{on} currents both underwent only minor changes, the greatest variation was observed for the device in the On-state mode, where I_{on} increased by

about 9% at 75 °C.

After trapping charges mainly in the AlGaN energy states due to TID of 350 krad, the DUTs showed little sensitivity to the effects of the temperature field. The values of V_{th} were shifted to smaller values, presenting a maximum variation of about 9% for the On-state at 50 °C and at −25 °C for the Off-state. Only in the Off-state, at 75 °C, the variation observed was slightly positive.

The maximum transconductance variation, Δgm_{max}, for both state-conditions (On/Off), was positive and decreased from −50 °C to room temperature (RT) of 21 °C, demonstrating a decrease in the mobility of the carriers that compose the electron gas as the temperature increased. For temperatures above RT, there was an increase in the electron mobility in the On-state, while a decrease was observed in the electron mobility in the Off-state. In all cases, however, fluctuations in gm_{max} induced by temperature did not exceed 2%.

5. Summary

The two main ways in which the effects of ionizing radiation affect the functionality of the 2DEG-based transistor are by changing the electronic density and/or modifying electronic mobility. Carrier concentration in a 2DEG is changed by charge trapping, causing changes in the electric field in the interface. Considering the accumulated positive charges of the AlGaN layer will increase the electric field at the interface, allowing a higher electronic density. If negative charge entrapment occurs at the interface, the electric field and resulting carrier density will decrease. On the other hand, if the positive and negative charges are trapped in the GaN layer, the effects on device operation will be exactly opposite, changing the threshold voltage. In addition, donor-type traps can be generated in both AlGaN and GaN layer, contributing to the increase in conduction electrons, ie, an increase in 2DEG concentration occurs [1–5,22]. The good behavior of these heterostructure field effect transistors (HFETs) both in the face of TID and temperature effects are mainly due to being a wide bandgap (WBG) device that drives carriers via 2DEG. Due to its band structure, electron tunnelling effects through the AlGaN-GaN interface are considered inherent to the transistor model. Electrons that tunnel through the Schottky barrier to the AlGaN conduction band have enough energy to pass from the AlGaN layer to the GaN layer by simple thermionic emission [39,40].

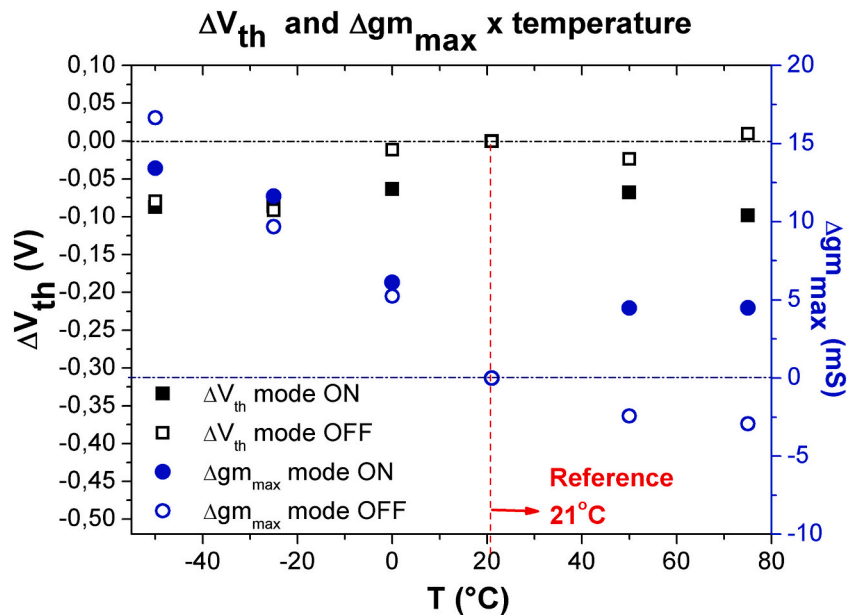The fact that the behavior of these devices brings better performance

Fig. 10. V_{th} and gm_{max} variations for temperatures between −50 °C and 75 °C. The variations were measured with respect to the room temperature (RT = 21 °C) established as reference.

operating in the On-state than in the Off-state is because in off mode the electric field is changed only vertically due to the voltage applied to the port to characterize the device during X-ray exposure. Thus, this vertical field that governs changes in 2DEG carrier concentration, mobility, and threshold voltage. In On mode, the device is initially polarized, influenced by vertical and horizontal electric field components. In this case, the electric field between source and drain must be considered, minimizing the effects of radiation on the dynamics of trapped charges.

6. Conclusions

GaN-HEMT, GS61008T - COTS, was analyzed in Off- and On-state mode showing an excellent recovery of functionality after TID of 350 krad, indicating to be less affected by the radiation when the device is on.

The greatest variation of V_{th} and gm_{max} were both obtained in the off-mode, and during irradiation: $\Delta V_{th}^{max} = -0.46$ V and $\Delta gm_{max}^{max} = -130$ mS, respectively. In addition, the best recovery of functionality after the 7 days of RTA was in the on-mode with $\Delta V_{th}^{RTA} = -0.05$ V and $\Delta gm_{max}^{RTA} = -45$ mS.

Although not conclusive, concerning to the maximum switching frequency, the radiation tests at low and high frequency, from 100 Hz to 100 kHz, allowed a comparative approach to the rise and fall times under the used operating conditions. The radiation effects for the DUT under 100 Hz showed minor changes, however, the effects for the DUT under 100 kHz presented considerable changes, which is more pronounced in the Off-state mode.

Regarding the temperature test, carried out after irradiation, even observing a decrease in the electron mobility in the Off-state. In all cases, however, fluctuations in gm_{max} induced by temperature did not exceed 2%.

Results of switching tests and temperature tolerance showed minor changes, which should not interfere with the performance of the device. So, all results confirm that devices based on this new GaN technology are quite robust to TID effects and good candidates to be used in hostile environments.

Declaration of competing interest

The authors declare that they have no known competing financial interests or personal relationships that could have appeared to influence the work reported in this paper.

Acknowledgments

References

[1] Muhammad Navid A.A. et al., High electron mobility transistors: performance analysis, research trend and applications. INTECH Open Sci. https://doi.org/10.5772/67796.

[2] Edward A. Jones, et al., Review of commercial GaN power devices andGaN-based converter design challenges, IEEE J. Emerg. Sel. Top. Power Elect. 4 (3) (Sept. 2016) 707–719.

[3] S.J. Pearton, et al., Review-ionizing radiation damage effects on GaN devices, ECS J. Solid State Sci. Tech. 5 (2) (2016) Q35–Q60.

[4] J. Jimenez, A. Moore, GaN RF Technology for Dummies, John. Wiley & Sons, Inc., Hoboken, 2014.

[5] A. Bindra, Wide-bandgap-based power devices: reshaping the power electronics landscape, IEEE Power Electron. Mag. 2 (1) (Mar. 2015) 42–47.

[6] Ke Li, et al., SiC/GaN power semiconductor devices: a theoretical comparison and experimental evaluation under different switching conditions, IET Elect. Syst. Transp. 8 (1) (2018) 3–11.

[7] Y. Nakasha, et al., E-band 85-mW oscillator and 1.3-W amplifier ICs using 0.12-μm GaN HEMTs for millimeterwave transceivers, in: 2010 IEEE Compound Semiconductor Integrated Circuit Symposium, 2010, pp. 1–4.

[8] S. Tirelli, et al., 107-GHz (Al,Ga)N/GaN HEMTs on silicon with improved maximum oscillation frequencies, IEEE Electron Device Lett. 31 (4) (April 2010) 296–298, https://doi.org/10.1109/LED.2009.203.

[9] Xiaoxu Cheng, et al., Physics-based compact model for AlGaN/GaN MODFETs with close-formed I–V and C–V characteristics, IEEE Trans. Electron. Devices 56 (12) (Dec. 2009) 2881.

[10] Asmae Babaya, et al., Analytic estimation of two-dimensional electron gas density and current-voltage, Int. J. Electr. Comp. Eng. (IJECE) 8 (2) (April 2018) 954–962.

[11] Y. Uemoto, et al., Gate injection transistor (GIT)—a normally-off AlGaN/GaN power transistor using conductivity modulation, IEEE Trans. Electron Devices 54 (12) (Dec. 2007) 3393–3399, https://doi.org/10.1109/TED.2007.908601.

[12] GS61008T Top-side cooled 100 V E-mode GaN transistor preliminary datasheet. GaN Systems. https://gansystems.com/wp-content/uploads/2018/04/GS61008T-DS-Rev-180420.pdf, 2018.

[13] R. Velazco, P. Fouillat, R. Reis, Radiation Effects on Embedded Systems, Springer, Dordrecht, NL, 2007.

[14] A. Johnston, Reliability and Radiation Effects in Compound Semiconductors, World Scientific Publishing Co. Pte. Ltd., California Institute of Technology, USA, 2010.

[15] James R. Schwank, et al., Radiation hardness assurance testing of microelectronic devices and integrated circuits: radiation nvironments, physical mechanisms and foundations for hardness assurance, in: Document 2008-6851P, Sandia National Laboratories, 2008.

[16] M. Rahman, et al., Super-radiation hard detector technologies: 3-D and Widegap detectors, IEEE Trans. Nucl. Sci. 51 (2004) 2256.

[17] N.W. Ashcroft, N.D. Mermin, Solid State Physics, Saunders, Philadelphia, 1976.

[18] H.Y. Xiao, F. Gao, X.T. Zu, W.J. Weber, Threshold displacement energy in GaN: ab initio molecular dynamics study, J. Appl. Phys. 105 (2009) 123527.

[19] B.D. Weaver, et al., Displacement damage effects in AlGaN/GaN high electron mobility transistors, IEEE Trans. Nucl. Sci. 59 (2012) 3077.

[20] M.A.G. Silveira, et al., Performance of electronic devices submitted to X-rays and high energy proton beams, Nucl. Inst. Methods Phys. Res. B Beam Interactions Mater. Atoms 273 (2012) 135–138.

[21] M.A.G. Silveira, et al., Radiation effect mechanisms in electronic devices, in: 10th Latin American Symposium on Nuclear Physics and Applications, SISSA, Montevideo, 2014.

[22] Jeffrey T. Moran, John W. McClory, James C. Petrosky, Gary C. Farlow, The effects of temperature and electron radiation on the electrical properties of AlGaN/GaN HFETs, IEEE Trans. Nucl. Sci. 56 (6) (Dec. 2009) 3223.

[23] M.J. Martinez, et al., Radiation response of AlGaN-channel HEMTs, IEEE Trans. Nucl. Sci. 66 (1) (Jan. 2019) 344–351, https://doi.org/10.1109/TNS.2018.2885526.

[24] X. Sun, et al., Total-ionizing-dose radiation effects in AlGaN/GaN HEMTs and MOS-HEMTs, IEEE Trans. Nucl. Sci. 60 (6) (Dec. 2013) 4074–4079, https://doi.org/10.1109/TNS.2013.2278314.

[25] R. Jiang, et al., Dose-rate dependence of the total-ionizing-dose response of GaN-based HEMTs, IEEE Trans. Nucl. Sci. 66 (1) (Jan. 2019) 170–176, https://doi.org/10.1109/TNS.2018.2873059.

[26] A. Lidow, A. Nakata, M. Rearwin, J. Strydom, A.M. Zafrani, Single-event and radiation effect on enhancement mode gallium nitride FETs, in: 2014 IEEE Radiation Effects Data Workshop (REDW), Paris, 2014, pp. 1–7, https://doi.org/10.1109/REDW.2014.7004594.

[27] R.D. Harris, et al., Radiation characterization of commercial GaN devices, in: 2011 IEEE Radiation Effects Data Workshop, Las Vegas, NV, 2011, pp. 1–5, https://doi.org/10.1109/REDW.2010.6062526.

[28] L.E. Seixas, et al., Study of proton radiation effects among diamond and rectangular gate MOSFET layouts, Mater. Res. Express 4 (2017), 015901.

[29] F.G.H. Leite, et al., Radiation effects on a COTS low-cost RISC microcontroller, in: 2017 18th IEEE Latin American Test Symposium (LATS), Bogota, 2017.

[30] M.R. Shaneyfelt, et al., Total ionizing dose and single event effects hardness assurance qualification issues for microelectronics, IEEE Trans. Nuclear Sci. 55 (4) (2008) 1926–1946.

[31] European Space Agency, ESCC basic specification no. 22900, total dose steady-state irradiation test method [Online]. Available: https://escies.org/, Jun. 2016.

[32] Test Method Standard Microcircuits, Standard MIL-STD-883K, Department of Defense [Online]. Available: https://landandmaritimeapps.dla.mil/Downloads/MilSpec/Docs/MIL-STD-883/std883mthd1000.pdf, 2017.

[33] NIST Standard Reference Database [Online]. Available: https://www.nist.gov/pml/x-ray-mass-attenuation-coefficients.

[34] F. Ravotti, Dosimetry techniques and radiation test facilities for total ionizing dose testing, IEEE Trans. Nucl. Sci. 65 (8) (Aug. 2018) 1440–1464, https://doi.org/10.1109/TNS.2018.2829864.

[35] GRANDEZAS RADIOLÓGICAS E UNIDADES [Online]. Available: https://inis.iaea.org/collection/NCLCollectionStore/_Public/45/073/45073470.pdf.

[36] Radiation Measurement [Online]. Available: www.radcal.com.

[37] 100V GaN E-HEMT half bridge evaluation kit, Available: https://gansystems.com/wp-content/uploads/2018/03/GS61008P-EVBHF-User-Guide-180227.pdf.

[38] A.C.V. Bôas, et al., Assessment of ionizing radiation hardness of a GaN field-effect transistor, in: 2019 34th Symposium on Microelectronics Technology and Devices (SBMicro), Sao Paulo, Brazil, 2019, pp. 1–4, https://doi.org/10.1109/SBMicro.2019.8919340.

[39] M.P. Khanal, et al., Impact of 100 keV proton irradiation on electronic and optical properties of AlGaN/GaN high electron mobility transistors (HEMTs), J. Appl. Phys. 124 (21) (2018), 215702.

[40] B.D. Weaver, et al., On the radiation tolerance of AlGaN/GaN HEMTs, ECS J. Sol. State Sci. Technol. 5 (7) (2016) Q208.